Robust quantum Griffiths singularity above 1.5 K in nitride thin films

Xiaoni Wang,[1,2] Lijie Wang,[3] Yixin Liu,[1,2] Fan Chen,[1,2] Wanpeng Gao,[1,2] Yu Wu,[1] Zulei Xu,[1,2] Wei Peng [1,2]
Zhen Wang,[1,2] Zengfeng Di,[1,2] Wei Li,[3,*] Gang Mu [1,2,†] and Zhirong Lin[1,2,‡]

[1]*State Key Laboratory of Functional Materials for Informatics, Shanghai Institute of Microsystem and Information Technology,*
Chinese Academy of Sciences, Shanghai 200050, China
[2]*College of Materials Science and Opto-electronic Engineering, University of Chinese Academy of Sciences, Beijing 100049, China*
[3]*Department of Physics and State Key Laboratory of Surface Physics, Fudan University, Shanghai 200433, China*

Quantum Griffiths singularity (QGS), which is closely correlated with the quenched disorder, is characterized by the divergence of the dynamical critical exponent when approaching zero temperature and the applicability of activated scaling. Typically such a phenomenon is rather rare and only observed in extremely low temperatures. Here we report the experimental observation of a robust QGS in NbN thin films, which survives in a rather high temperature range. The electrical transport properties were measured under the magnetic field up to 12 T. The field induced superconductor-metal transitions were observed with the continuously changed transition points with the decrease of temperature. The dynamical critical exponent based on the conventional power-law scaling reveals a divergent trend when approaching the low-temperature limit. Moreover, the temperature and field dependence of sheet resistance can be described by the activated scaling analysis in the temperature region up to $1.6 \text{ K} \leqslant T \leqslant 4.0 \text{ K}$. We argue that the robustness of QGS in the present system originates from the pronounced Pauli paramagnetic effect due to the strong coupling between magnetic field and the spin degree of freedom of the superconducting electrons.

I. INTRODUCTION

The phase transition between different ground states, which is accompanied by quantum rather than thermal fluctuations, is called the quantum transition [1,2]. For example, the superconductor-insulator transition (SIT) is typically driven by disorder, magnetic field (B), or carrier concentration [3–8]. Such a quantum transition can have a significant influence on the physical performance in finite temperatures in terms of the quantum fluctuations. In the conventional scenes, only one critical transition point exists and the temperature dependent resistance (R) near the SIT point can be described by a power-law scaling determined by the critical exponents (z, ν) and the distance from the critical point [9–13]. Recently, it was reported that, in the two-dimensional (2D) or quasi-2D systems with quenched disorder, a new type of superconductor-metal transition (SMT) emerges. In these systems, the crossing point in the $R(B)$ curves can reveal a systematic variation with temperature and the effective critical exponent at each crossing point shows a divergent behavior when approaching zero temperature [14–20].

It was interpreted that [21,22], due to the transformation of the vortex lattice into the vortex glasslike phase in the zero-temperature limit, rare regions of inhomogeneous superconducting (SC) islands (or puddles) gradually show up in the high field regime. As a result, the quantum Griffiths singularity emerges, which manifests an activated scaling behavior in a limited temperature range. It is believed [14] that such a vortex glasslike phase is rather delicate against the thermal fluctuation since, in the high-temperature region, thermal fluctuations will smear the inhomogeneity caused by quenched disorder. Thus, the rare regions of the SC islands could not exist. In other words, the quantum Griffiths singularity can only be observed in extremely low temperatures, where the impact of quenched disorder overtakes thermal fluctuations. Indeed, almost all the QGS behaviors in the previous reports occurred in extremely low temperatures. However, it was found that QGS can exist in a relatively high temperature region of 4 to 5 K in ion-gated ZrNCl system [17]. This issue has not been fully noticed and discussed. Theoretically, it has been pointed out [22] that the domination of spin-related pair-breaking effect will lead to a larger energy associated with the formation of the SC puddles. Currently there is still a lack of thorough investigations concerning the upper limit of temperature that QGS can survive.

In this study, we conducted an in-depth investigation on the field induced superconductor-metal transition in NbN thin films, whose SC critical temperature T_c has been tuned to below 4 K. Systematic variations of the crossing points B_x and the effective critical exponents $z\nu$ were observed in a finite temperature range. Moreover, the temperature and field dependence of sheet resistance can be described by the activated dynamical scaling in a relatively wide temperature region up to 4 K. Our finding indicates that the features of the quantum

---

*w_li@fudan.edu.cn
†mugang@mail.sim.ac.cn
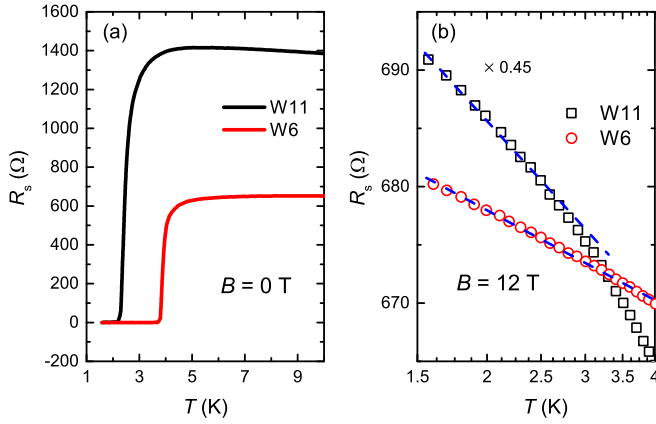‡zrlin@mail.sim.ac.cn

094509-1

FIG. 1. Temperature dependence of sheet resistance R_s under the magnetic fields of 0 T (a) and 12 T (b) for two samples. The semi logarithmic coordinates is used in (b). The blue dashed lines are visual guides.

Griffiths singularity actually can survive in high temperatures in the presence of strong Pauli paramagnetic effect.

II. MATERIALS AND METHODS

The NbN thin films were deposited using the method of DC reactive magnetron sputtering. The details of the conditions for the film growth have been reported previously [23]. We note that the NbN films are nonepitaxial, since the high-resistivity Si was used as the substrate. In the present work, two films (W11 and W6) deposited under different chamber pressures, 0.20 and 0.13 Pa respectively, were chosen to conduct the following investigations. The thicknesses of the two films are 25 and 20 nm respectively, as determined by the x-ray reflectivity measurements. The films were etched into the line shape with the dimension 10×500 μm^2 using reactive ion etching to conduct the electrical transport measurements.

The electrical transport measurements were performed using a cryostat (Oxford Instruments TeslatronPT cryostat system) with the field of up to 12 T. The applied electric current is 0.5 μA during the transport measurements. The magnetic field was applied perpendicular to both the film surface and the direction of electrical current.

III. RESULTS

The sheet resistance R_s as a function of temperature of the two samples is shown in Fig. 1. Under zero field, as shown in Fig. 1(a), clear SC transitions can be seen in the R_s-T curves, with the T_c of 2.5 K and 3.9 K for samples W11 and W6, respectively. Here the values of T_c are defined as the temperature where the sheet resistance becomes half of the normal-state value. Besides the superconductivity, the magnitude of sheet resistance in the normal state just above T_c, R_N, also reveals a clear difference between the two samples: $R_N = 1400$ and 650 Ω for W11 and W6, respectively. It is notable that the R_s-T curve under a high field of 12 T shows a logarithmic temperature dependence in the low temperature region, see Fig. 1(b). This feature is the hallmark of the 2D quantum-corrected disordered metal, where weak localization

TABLE I. Important parameters of the two samples.

Name	T_c (K)	R_N (Ω)	B_c (T)	$\nu\psi$	T_0 (K)
W11	2.5	1400	7.50	0.60 ± 0.03	6.0
W6	3.9	650	9.60	0.55 ± 0.02	9.1

plays a crucial role in determining the nature of electrons [18,24].

In order to investigate the detailed characteristic of this field induced transition from SC to the metallic state, we measured the temperature dependence of R_s under a series of magnetic fields up to 12 T. In Fig. 2, we display the data of sample W11. As shown in Fig. 2(a), with the increase of field, the steep descent behavior due to the SC transition is suppressed gradually, and eventually turns into a quantum-corrected metallic state. By carrying out a matrix inversion [18] of the temperature-swept data (see Fig. S1 in the Supplemental Material (SM) [25] where the situation of sample W6 is taken as an example), field dependence of R_s can be generated, which is shown in Fig. 2(b). A series and continuum of crossings in the R_s-B curves can be seen, which spread out over a wide range of temperatures (1.6–5 K) and magnetic field. This is very different from the conventional quantum phase transition where only one crossing point exists [26] and stresses the importance of certain energy scales in this system with quenched disorder. Thus, the conventional power-law scaling could not describe this behavior on the whole. We extracted the positions of the crossing points B_x and showed them in Fig. 2(c) as a function of temperature. The value of the temperature corresponding to each crossing point is determined by averaging the temperatures of the two isotherms that generate the crossing. It was pointed out [18] that, as expected near an infinite-randomness critical point, the evolution of B_x with temperature can be simulated using the equation

$$B_x(T) = B_c \times \left[1 - u \left(ln \frac{T_0}{T} \right)^{-p} \right], \tag{1}$$

where B_c and T_0 are the critical field in the zero-temperature limit and a microscopic temperature scale, respectively. u and p are fitting parameters. Similar to the fitting process adopted in the literature [18], B_c, u, and p are set as free parameters, while T_0 is fixed as the value determined from the fit in Fig. 3 (see Table I). The fitting result is presented by the blue solid line in Fig. 2(c).

Similar to the previous reports in other systems [14,18–20], despite the inappropriateness in describing the R_s-B data on the whole, the conventional power-law scaling can still be used to analyze the data in each small temperature intervals, which is expressed as [26]

$$R_s(\delta_x, T) = F(\delta_x T^{-1/z\nu}), \tag{2}$$

where $\delta_x = |B - B_x|/B_x$ is the normalized distance from the effective critical field B_x in each small temperature range, ν is the correlation-length exponent, z is the dynamical-scaling exponent, and F is the scaling function with $F(0) = 1$. The results of the scaling using Eq. (2) are shown in Figs. S2 and
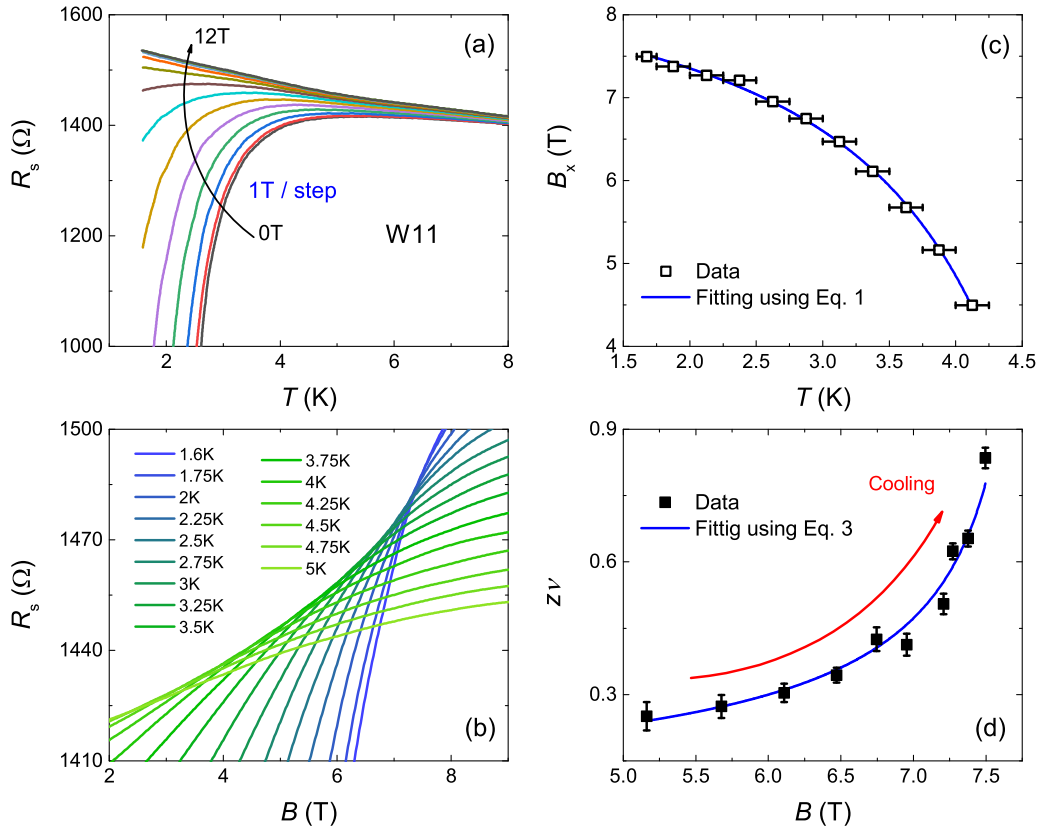
FIG. 2. (a) Temperature dependence of sheet resistance under magnetic fields up to 12 T for sample W11. (b) Field dependence of sheet resistance at temperatures ranging from 1.6 K to 5 K. (c) Crossing points from the magnetoresistance isotherms shown in (b). The error bars represent the sizes of temperature intervals of the two R_s-B curves which determine the position of B_x. The blue solid line is a fit to Eq. (1) (see text). (d) Field dependence of the critical exponent $z\nu$ obtained from finite size scaling analysis. The error bars in $z\nu$ values are determined by examining the influence of critical exponents on the standard deviation of scaling behavior. The blue solid line shows the fitting curve based on the activated scaling law.

S3 in the SM [25]. The obtained critical exponents $z\nu$ as a function of field are shown in Fig. 2(d). With the decrease

FIG. 3. Sheet resistance as a function of scaling variable $\delta[\ln(T_0/T)]^{1/\nu\psi}$ in the temperature range 1.6 K $\leqslant T \leqslant$ 3.5 K. The red dashed lines are visual guides.

of temperature, the value of $z\nu$ reveals an upward trend with an increasing steepness. Such a divergent tendency is the hallmark of the activated dynamical scaling [14], which can be simulated using the following equation:

$$z\nu = C \times |B - B_c|^{-\nu\psi}, \qquad (3)$$

where C is a constant. ν and ψ are the correlation-length exponent and the tunneling exponent, respectively. It has been estimated theoretically [27] that $\nu = 1.2$ and $\psi = 0.5$. Thus, the power exponent is set as $\nu\psi = 0.6$ in the fitting process, similar to that used by other groups [14,20]. As shown by the blue solid line in Fig. 2(d), the experimental data, especially the divergent tendency in the low temperature region, can be well described by Eq. (3).

Theoretically, quantum Griffiths singularity is closely related to the infinite-randomness critical point. As we have mentioned above, the quantum SMT governed by such an infinite-randomness fixed point could not be described by the conventional power-law scaling on the whole. Actually, the activated dynamical scaling has been proposed [18,28] in the following form:

$$R_s\left(\delta, \ln\frac{T_0}{T}\right) = \Phi\left[\delta\left(\ln\frac{T_0}{T}\right)^{1/\nu\psi}\right]. \qquad (4)$$
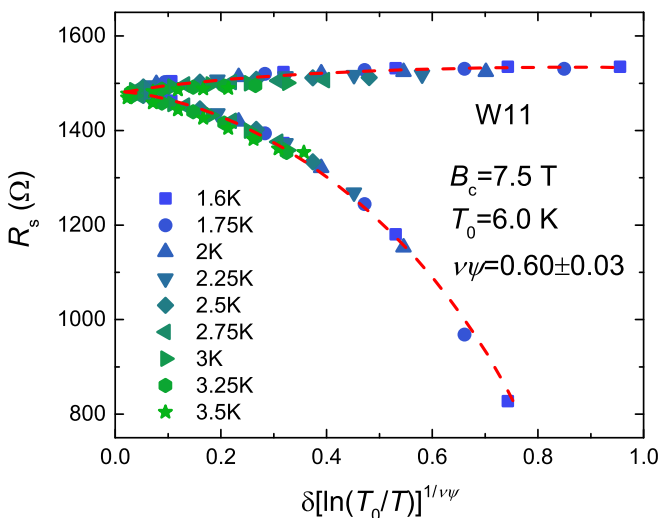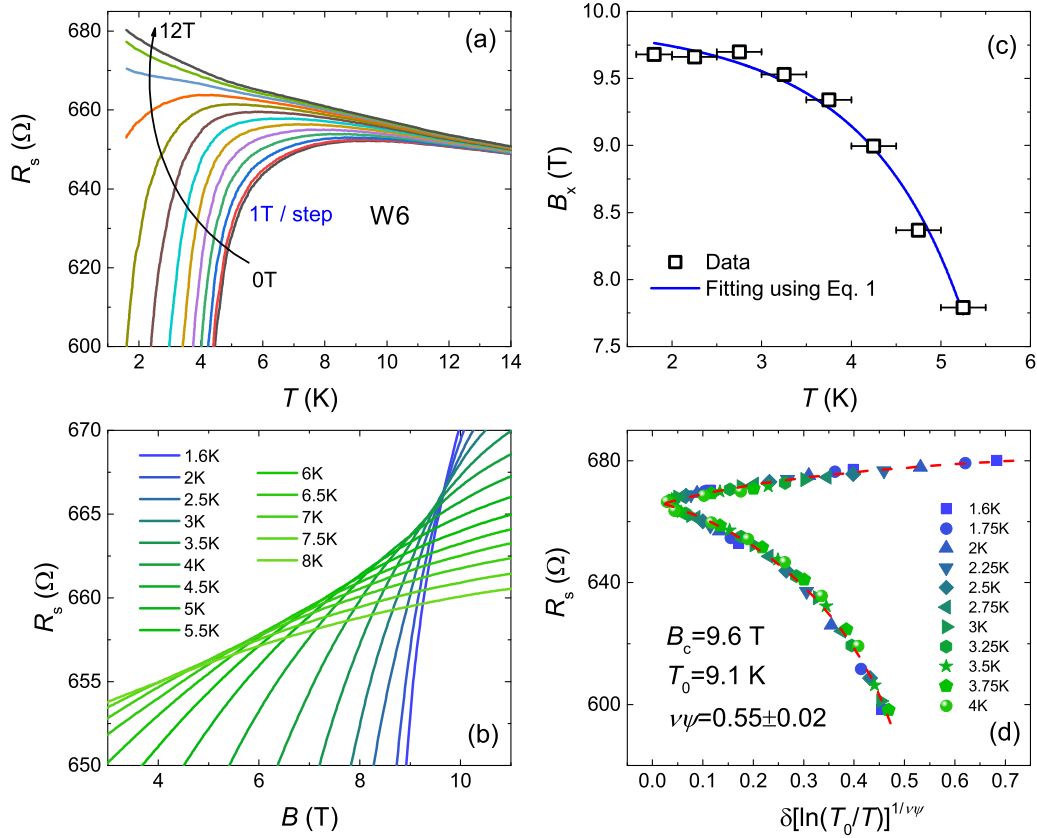
FIG. 4. (a) Temperature dependence of sheet resistance under magnetic fields up to 12 T for sample W6. (b) Field dependence of sheet resistance at temperatures ranging from 1.6 K to 8 K. (c) Crossing points from the magnetoresistance isotherms shown in (b). The blue solid line is a fit to Eq. (1) (see text). (d) Sheet resistance as a function of scaling variable $\delta[\ln(T_0/T)]^{1/\nu\psi}$ in the temperature range 1.6 K $\leqslant T \leqslant$ 4 K. The red dashed lines are visual guides.

Here $\delta = |B - B_c|/B_c$ is the normalized distance from the critical field B_c. Φ is the function of the activated dynamical scaling. According to this equation, there is only one single crossing point in magnetic field, which does not account for the temperature dependence of the crossing fields in the experimental data. In Fig. 3, we show the result of the activated dynamical scaling according to Eq. (4). All the experimental data in the temperature range 1.6 K $\leqslant T \leqslant$ 3.5 K collapse into a single curve, indicating the rationality of the activated dynamical scaling in describing our data. From this scaling, the critical exponent $\nu\psi = 0.60 \pm 0.03$ and critical field $B_c = 7.50$ T were obtained.

Sample W6, with a relatively higher T_c and lower R_N, also reveals the field induced SMT, as shown in Fig. 4(a). Similar to that observed in sample W11, the crossing points in the R_s-B curves experience a series of evolution with temperature, which tends to be saturated at above 9 T as the temperature goes toward lower temperatures [see Fig. 4(b)]. The values of the crossing fields B_x are recorded in Fig. 4(c), from which the saturated tendency can be seen more clearly. Again the B_x-T data are simulated using Eq. (1) as revealed by the blue solid line in Fig. 4(c). The temperature and field dependence of sheet resistance in the temperature range 1.6 K $\leqslant T \leqslant$ 4.0 K is analyzed using the activated dynamical scaling, which are shown in Fig. 4(d). The scaling parameters are $B_c = 9.6$ T, $\nu\psi = 0.55 \pm 0.02$, and $T_0 = 9.1$ K. The parameters of the two samples are summarized in Table I to have a comparison.

We note here that the values of $\nu\psi$ for the two samples are in a reasonable range for a two-dimensional infinite-randomness critical point in the random transverse-field Ising model [27].

IV. DISCUSSION

The adjustability in a large range in the physical properties of NbN films [23,29,30] provides convenience to broaden the extension of ground state in investigating the quantum phenomena, such as the QGS in field induced SMT. In this work, the sheet resistance in the normal state is tuned from 1400 Ω to 650 Ω. Our results suggest that the quantum Griffiths singularity can be observed in the system with R_N being suppressed to half. In the case of PdTe$_2$ films [20], the feature of QGS disappears under perpendicular field when R_N is reduced to the value below 200 Ω by increasing the film thickness. Finding and determining the critical point of where QGS disappears are of great significance for revealing the essence of this quantum phenomenon. Based on the present NbN system, we can systematically adjust its normal-state resistance without changing the film thickness, so that the boundary of the QGS state can be accurately determined. This will be the next step of our work. On the other hand, based on the random transverse-field Ising model [31], the values of the critical exponent $\nu\psi$ can be affected by the detailed form or strength of the disorder. Thus the difference in the value of $\nu\psi$
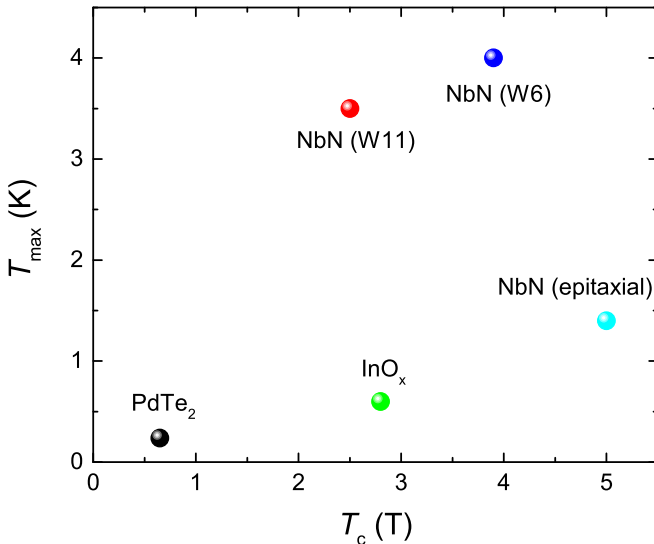
FIG. 5. The maximum temperature T_{max} in the activated dynamical scaling [Eq. (4)] as a function of the mean field superconducting transition temperature T_c. The data from InO_x [18], $PdTe_2$ [20], and epitaxial NbN film [32] are also shown for a comparison.

FIG. 6. B-T phase diagram for the NbN system, taking sample W6 as an example. The black diamonds and olive balls represent the mean field upper critical field B_{c2} and the crossing points B_x of the R_s-B curves, respectively. The red curve is the fitting result based on the Werthamer-Helfand-Hohenberg model.

between the two samples actually reflects the variation of the detailed situation of the quenched disorder.

Another important issue worth our attention is the temperature range where QGS occurs. Based on the general understanding [14], QGS is rather delicate against the thermal fluctuation, since the inhomogeneity caused by quenched disorder can be smeared by the thermal fluctuations in the high-temperature region. In this case, the rare regions of the SC islands (puddles) could hardly survive. In our work, however, it is found that the activated dynamical scaling can describe the electrical transport data in the temperature range $1.6\,\mathrm{K} \leqslant T \leqslant 3.5\,\mathrm{K}$ (see Fig. 3) or $1.6\,\mathrm{K} \leqslant T \leqslant 4.0\,\mathrm{K}$ [see Fig. 4(d)]. In order to have an intuitive comparison, we show the maximum temperature T_{max} in the activated dynamical scaling [Eq. (4)] as a function of T_c in Fig. 5. It can be seen that for InO_x [18], $PdTe_2$ [20], and epitaxial NbN film [32], T_{max} is several times lower than T_c. While for the nonepitaxial NbN films in the present work, T_{max} is at the same level as T_c. This can be seen more clearly in the B-T phase diagram, as shown in Fig. 6. The region of the quantum Griffiths state enclosed by the orange dashed line is more pronounced than that in other systems [17,32].

Theoretically, the size, distance, and concentration of the SC puddles are important parameters in controlling the performance of the QGS [22]. These factors determine the coupling strength between optimal puddles. Moreover, in the magnetic field induced SMT, the modes of coupling between the field and the SC state can also play an important role, which may give rise to a different microscopic physics responsible for the emergence of the puddle state. It was pointed out [22] that, in the case that the coupling of the applied magnetic field to the electron spin (Zeeman coupling) is significant and the spin-orbit coupling is weak, the superconductor-metal transition tends to be first order on the mean field level. As a result, the energy associated with the formation of puddles is obviously enhanced and the puddle state should be more
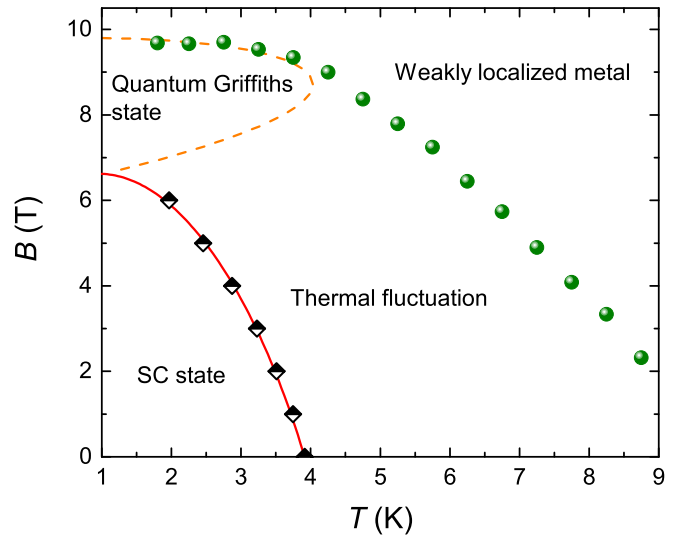
robust. Although the authors of Ref. [22] took the case of thin film with a parallel magnetic field as an example, there is another situation that meets this condition. In our previous work [23], we have uncovered a pronounced Pauli paramagnetic effect in the present NbN system. As shown in Fig. S4, temperature dependence of B_{c2} for W6 was fitted based on the Werthamer-Helfand-Hohenberg model, which gives a rather large Maki parameter of $\alpha = 2.1$. This emphasizes the significant influence of the coupling between the magnetic field and spin degree of freedom in the present system. We argue that this is the most probable reason why we have observed such a robust QGS state in the nonepitaxial NbN films. We note that, compared with the present nonepitaxial system, epitaxial NbN film reveals a clearly different behavior and the value of T_{max} is much lower [32]. It is beneficial and necessary to further analyze this difference. We have pointed out [23] that the strength of the Pauli paramagnetic effect is closely correlated with the slope of the upper critical field near T_c, $B^* = -dB_{c2}(T)/dT \,|_{T_c}$, which is 7.5 and 5.5 T/K for samples W11 and W6, respectively. An estimation shows that the value of B^* is below 2 T/K for the epitaxial NbN film [32], indicating a weaker Pauli paramagnetic effect. Obviously, this sharp contrast is consistent with our above speculation.

V. CONCLUSIONS

In summary, we studied the field induced superconductor-metal transition in the nonepitaxial NbN thin films. The quantum Griffiths singularity, in terms of the systematical evolution of the crossing point B_x in the R_s-B curves and the applicability of the activated scaling analysis to the transport data, was observed in two samples with different T_c and R_N. Significantly, activated scaling can be valid in the temperature range as high as 1.6 K to 4.0 K, revealing the robustness of the QGS in the present system. Our analysis indicates that the strong Pauli paramagnetic effect plays a key role in enhancing

the stability of the puddle state, which is the precondition for the formation of QGS.

[1] M. Imada, A. Fujimori, and Y. Tokura, Rev. Mod. Phys. **70**, 1039 (1998).

[2] V. F. Gantmakher and V. T. Dolgopolov, Phys. Usp. **53**, 1 (2010).

[3] N. Marković, C. Christiansen, and A. M. Goldman, Phys. Rev. Lett. **81**, 5217 (1998).

[4] A. Yazdani and A. Kapitulnik, Phys. Rev. Lett. **74**, 3037 (1995).

[5] J. Biscaras, N. Bergeal, S. Hurand, C. Feuillet-Palma, A. Rastogi, R. C. Budhani, M. Grilli, S. Caprara, and J. Lesueur, Nat. Mater. **12**, 542 (2013).

[6] Y. Sun, H. Xiao, M. Zhang, Z. Xue, Y. Mei, X. Xie, T. Hu, Z. Di, and X. Wang, Nat. Commun. **9**, 2159 (2018).

[7] R. Schneider, A. G. Zaitsev, D. Fuchs, and H. v. Löhneysen, Phys. Rev. Lett. **108**, 257003 (2012).

[8] T. Wang, A. Yu, Y. Liu, G. Gu, W. Peng, Z. Di, D. Jiang, and G. Mu, Phys. Rev. B **106**, 104509 (2022).

[9] A. T. Bollinger, G. Dubuis, J. Yoon, D. Pavuna, J. Misewich, and I. Bozović, Nature (London) **472**, 458 (2011).

[10] X. Leng, J. Garcia-Barriocanal, S. Bose, Y. Lee, and A. M. Goldman, Phys. Rev. Lett. **107**, 027001 (2011).

[11] M. Liao, Y. Zhu, J. Zhang, R. Zhong, J. Schneeloch, G. Gu, K. Jiang, D. Zhang, X. Ma, and Q. K. Xue, Nano Lett. **18**, 5660 (2018).

[12] F. Wang, J. Biscaras, A. Erb, and A. Shukla, Nat. Commun. **12**, 2926 (2021).

[13] Y. Yu, L. Ma, P. Cai, R. Zhong, C. Ye, J. Shen, G. Gu, X. H. Chen, and Y. Zhang, Nature (London) **575**, 156 (2019).

[14] Y. Xing, H.-M. Zhang, H.-L. Fu, H. Liu, Y. Sun, J.-P. Peng, F. Wang, X. Lin, X.-C. Ma, Q.-K. Xue *et al.*, Science **350**, 542 (2015).

[15] S. Shen, Y. Xing, P. Wang, H. Liu, H. Fu, Y. Zhang, L. He, X. C. Xie, X. Lin, J. Nie *et al.*, Phys. Rev. B **94**, 144517 (2016).

[16] Y. Xing, K. Zhao, P. Shan, F. Zheng, Y. Zhang, H. Fu, Y. Liu, M. Tian, C. Xi, H. Liu *et al.*, Nano Lett. **17**, 6802 (2017).

[17] Y. Saito, T. Nojima, and Y. Iwasa, Nat. Commun. **9**, 778 (2018).

[18] N. A. Lewellyn, I. M. Percher, J. Nelson, J. Garcia-Barriocanal, I. Volotsenko, A. Frydman, T. Vojta, and A. M. Goldman, Phys. Rev. B **99**, 054515 (2019).

[19] X. Han, Y. Wu, H. Xiao, M. Zhang, M. Gao, Y. Liu, J. Wang, T. Hu, X. Xie, and Z. Di, Adv. Sci. **7**, 1902849 (2020).

[20] Y. Liu, S. Qi, J. Fang, J. Sun, C. Liu, Y. Liu, J. Qi, Y. Xing, H. Liu, X. Lin *et al.*, Phys. Rev. Lett. **127**, 137001 (2021).

[21] T. Vojta, J. Low Temp. Phys. **161**, 299 (2010).

[22] B. Spivak, P. Oreto, and S. A. Kivelson, Phys. Rev. B **77**, 214523 (2008).

[23] X. Wang, L. Wang, Y. Liu, W. Gao, Y. Wu, Z. Xu, H. Jin, L. Zhang, W. Peng, Z. Wang *et al.*, Physica C **606**, 1354223 (2022).

[24] B. Kramer and A. MacKinnon, Rep. Prog. Phys. **56**, 1469 (1993).

[25] See Supplemental Material at http://link.aps.org/supplemental/10.1103/PhysRevB.107.094509 for the results of the matrix inversion of the R_s-T data and the scaling using the conventional power-law relation [Eq. (2)].

[26] S. L. Sondhi, S. M. Girvin, J. P. Carini, and D. Shahar, Rev. Mod. Phys. **69**, 315 (1997).

[27] I. A. Kovács and F. Iglói, Phys. Rev. B **82**, 054437 (2010).

[28] A. Del Maestro, B. Rosenow, J. A. Hoyos, and T. Vojta, Phys. Rev. Lett. **105**, 145702 (2010).

[29] G. Oya and Y. Onodera, J. Appl. Phys. **45**, 1389 (1974).

[30] Z. Wang, A. Kawakami, Y. Uzawa, and B. Komiyama, J. Appl. Phys. **79**, 7837 (1996).

[31] F. lglói and C. Monthus, Phys. Rep. **412**, 277 (2005).

[32] T. Jing, Z. Han, Z. He, M. Shao, P. Li, and Z. Li, arXiv:2211.05001.